Electronic Supplementary Material (ESI) for Nanoscale.

Supporting information

Monolayer MBenes: Prediction of anode materials for high-performance lithium/sodium ion batteries

Jun Jia, BiJun Li, Shengquan Duan, Zhao Cui, Hongtao Gao*

State Key Laboratory Base of Eco-Chemical Engineering, College of Chemistry and Molecular Engineering, Qingdao University of Science & Technology, Qingdao, 266042, P. R. China.

*Address correspondence to gaohtao@qust.edu.cn.

Method Section

Cohesive energy: The cohesive energy is a recognized parameter for evaluating the feasibility of experimentally synthesizing predicted two-dimensional materials.[1] The cohesive energy for MBenes can be calculated by Eq. S1.

$$E_{Coh} = \frac{xE_M + yE_B - E_{M_xB_y}}{x + y} \quad \text{(S1)}$$

where E_M and E_B are the total energies of the separated transition metal and B atoms, respectively, and $E_{M_xB_y}$ is the total energy of the original MBene. A positive value indicates that the system is stable, and the larger the value is, the more stable the system.

Phonon dispersion curve: The dynamic stability of 2D MBenes is verified by the phonon spectra calculated with the PHONOPY code[2] on the basis of density functional perturbation theory (DFPT), in which a 5×5×1 supercell containing 100 atoms and a 4×4×1 K-point grid are employed.

AIMD simulation: The stability of MBenes (M=V, Cr, Mn) was evaluated by the Born-Oppenheimer approximation ab-initio molecular dynamics (AIMD) simulation method. The AIMD simulations were performed at 300 K using VASP with NVT integration.[3] All dynamic simulations lasted for 10 ps with a time step of 1.0 fs. Brillouin zone integration was applied using a 1×1×1 k-point grid during AIMD simulations.

Elastic properties: Both the Young's modulus and Poisson's ratio were calculated to describe the mechanical properties of the monolayer MBenes. The Young's modulus is a mechanical property that describes the resistance of solid materials to deformation and is defined as the relationship between the stress and the uniaxial deformation in the uniaxial elastic deformation region of a material within the scope applicable to Hooke's law. The Poisson's ratio is often used to estimate the expansion of materials in directions perpendicular to the direction of compression.

For a 2D crystal, the relationship between the elastic constant and the Young's modulus under plane stress can be obtained according to Hooke's law, which contains four

independent elastic constants that can be expressed by Eq. S2.[4]

$$C_{ij} = \begin{bmatrix} C_{11} & C_{12} & 0 \\ C_{12} & C_{22} & 0 \\ 0 & 0 & C_{66} \end{bmatrix} \quad (S2)$$

Based on the obtained elastic constants, the expressions of the direction-dependent Young's modulus y(θ) and Poisson's ratio ν(θ) are derived as follows[5] (θ is the angle along the α direction):

$$Y(\theta) = \frac{C_{11}C_{22} - C_{12}^2}{C_{11}s^4 + C_{22}c^4 + \left(\frac{C_{11}C_{22} - C_{12}^2}{C_{66}} - 2C_{12}\right)c^2s^2} \quad (S3)$$

$$\nu(\theta) = \frac{C_{12}(s^4 + c^4) + (C_{11} + C_{22} - \frac{C_{11}C_{22} - C_{12}^2}{C_{66}})c^2s^2}{C_{11}s^4 + C_{22}c^4 + \left(\frac{C_{11}C_{22} - C_{12}^2}{C_{66}} - 2C_{12}\right)c^2s^2} \quad (S4)$$

with s=sin(θ) and c=cos(θ).

Li/Na adsorption

We performed a full geometry optimization of MBenes with lithium/sodium molecules using a 3×3×1 supercell. The adsorption energy of lithium/sodium atoms on the MBene monolayer can be obtained by Eq. S5.

$$E_{ad} = \frac{(E_{MBene+nM} - E_{MBene} - nE_M)}{n} \qquad M=(Li, Na) \quad (S5)$$

Where $E_{MBene+nM}$ is the total energy of metallization for the MBene, E_{MBene} represents the total energy of the original MBene, and E_M is the total energy of the bulk metal.

To evaluate the adsorption stability of the Li/Na layer on the MBene monolayer, the average adsorption energy of each layer is calculated as follows.

$$E_{ave} = \frac{(E_{MBene+nM} - E_{M(n-1)MBene} - 8E_M)}{8} \qquad M=(Li, Na) \quad (S6)$$

where $E_{MBene+nM}$ and $E_{M(n-1)MBene}$ are the total energy of MBenes with n and (n-1) layers of

adsorbed Li/Na atoms, respectively, Em represents the total energy of each atom of the bulk metal, and "8" represents eight lithium/sodium atoms adsorbed in each layer (for a 2×2 supercell on both sides).

Theoretical specific capacitance

The adsorption of Li/Na at higher concentrations was calculated using a 2×2×1 supercell. The theoretical specific capacitance (C) of Li/Na-intercalated MBene can be estimated by Eq. S7.

$$C = \frac{nZ_A F}{M_{MBene} + nM} \qquad M = (Li, Na) \tag{S7}$$

where n is the number of metal atoms adsorbed; for Li, n = 24, and for Na, n = 16. F is the Faraday constant (26801 mA h/mol), M_{MBene} is the molar weight of the MBene, and M is the molar weight of the metal atoms.

Open-circuit voltage

For each concentration n of the $E_{MBene+nM}$ compound, the average open-circuit voltage (OCV) relative to M/M^+ is expressed as follows.

$$OCV_{ave} = \frac{E_{MBene} + nE_M - E_{MBene+nM}}{nzF} \tag{S8}$$

where n is the number of metal atoms adsorbed, E_M is the total energy of lithium/sodium atoms in the bulk metal, F is the Faraday constant (26801 mA h/mol), and Z is the charge of lithium ions in the electrolyte (z=1).

Figure captions

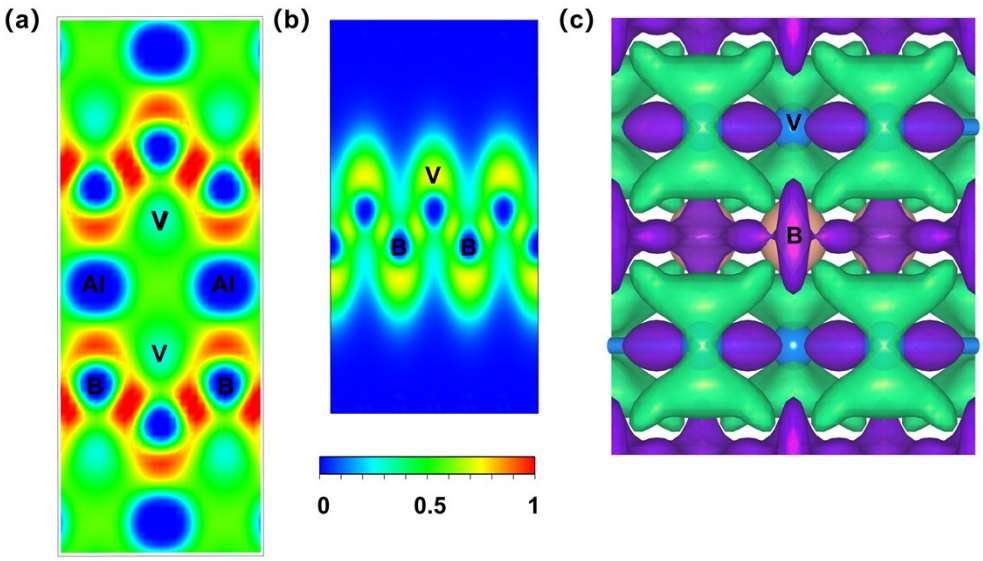

Fig. S1 (a) Electron localized function (ELF) contour plots projected on the [0001] plane for the V-Al bond and V-B bond. (b) ELF contour projected on the [0001] plane for the V-B bond after stripping. (c) Deformed electron density of monolayer V_2B_2, with an isosurface of 0.01 e·Å^{-3}. The green and purple areas represent the accumulation and depletion of electrons, respectively.

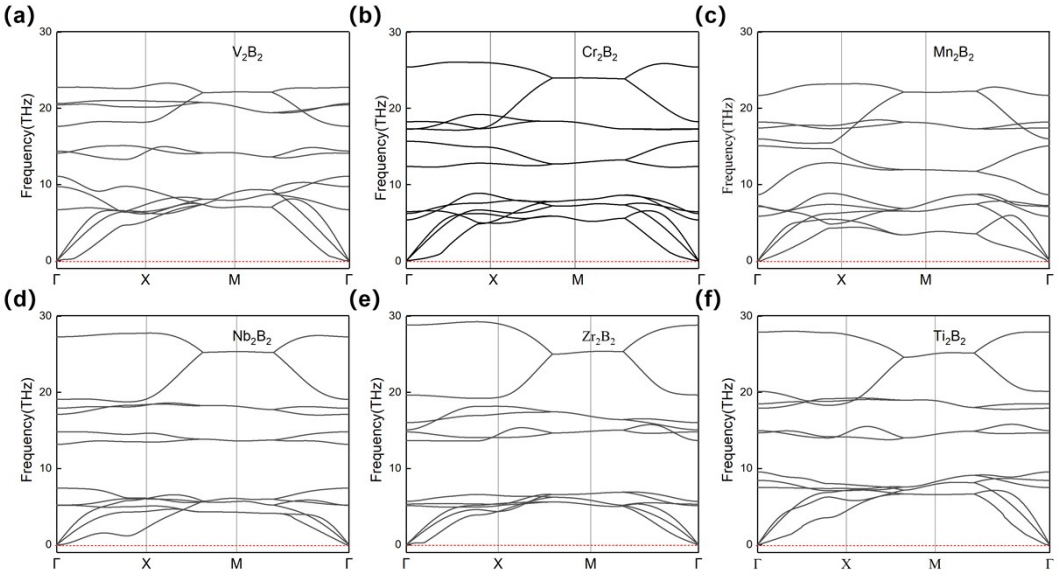

Fig. S2 Phonon dispersion curves of monolayer MBenes (V_2B_2, Cr_2B2, Mn_2B_2, Nb_2B_2, Zr_2B_2, Ti_2B_2).

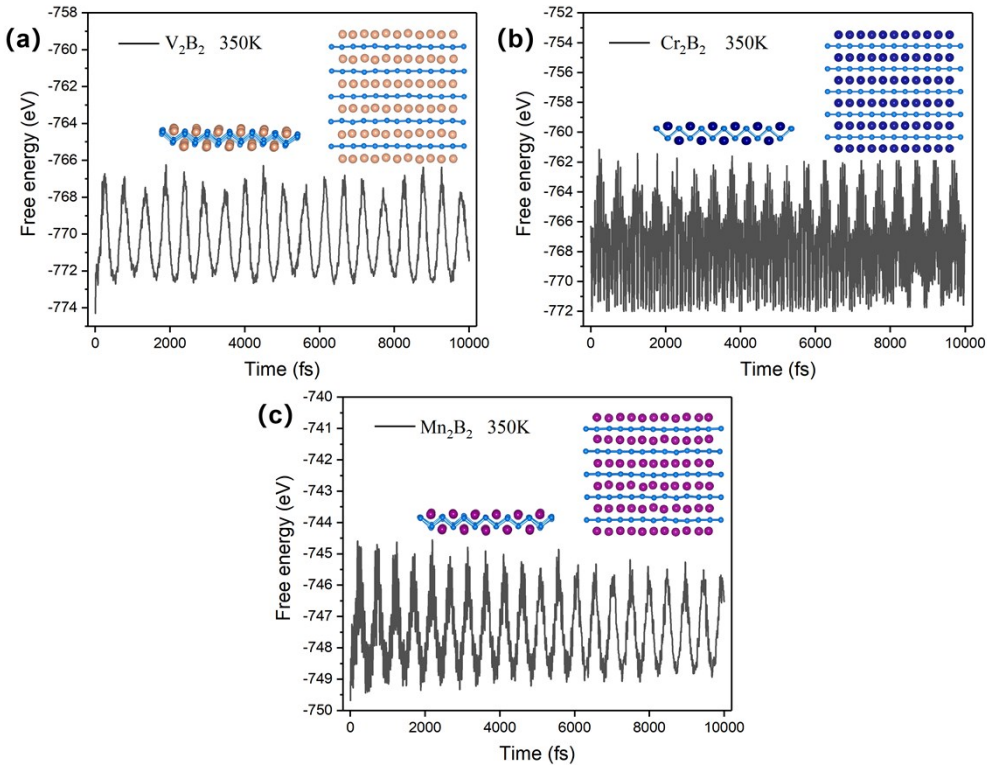

Fig. S3 At a temperature of 350 K, monolayer MBene (V_2B_2, Cr_2B_2, Mn_2B_2) molecular dynamics simulation snapshot. Free energy change trends and molecular dynamics simulation geometry.

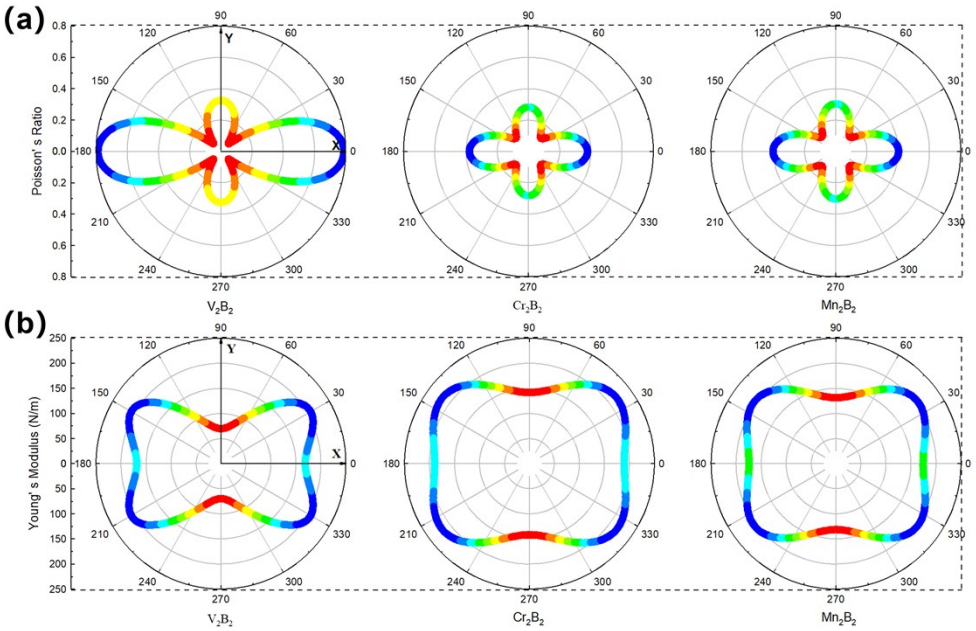

Fig. S4 Polar diagrams of (a) Young's modulus E(θ) and (b) Poisson's ratio for 2D V_2B_2, Cr_2B_2 and Mn_2B_2 MBenes.

For an orthogonal lattice, using an elastic constant in any direction specified by the polar angle θ (here, θ is the angle relative to the a direction), the in-plane Young's modulus Y and Poisson's ratio ν can be calculated by Eqs. S3 and S4. The polar map of MBenes (M=V, Cr, Mn) is shown in Fig. S3. In this figure, completely isotropic elastic behavior is represented by a perfect circle of Y and ν. In contrast, the shapes in Fig. S4(a) and Fig. S4(b) are highly anisotropic, especially that of V_2B_2, which is extended along the X-axis, and the Y-axis difference is significant, indicating that V_2B_2 has extremely strongly anisotropic mechanical properties.

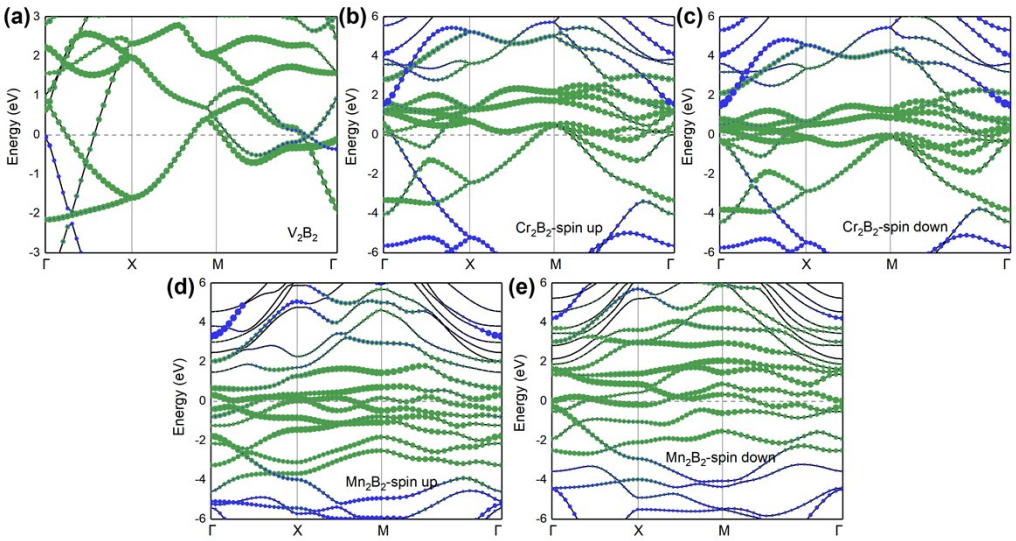

Fig. S5 Calculating a two-dimensional projection MBenes(V_2B_2, Cr_2B_2, Mn_2B_2) atomic energy band structure in which green and blue circles indicate the weights d orbital V / Cr / Mn and a p-orbital of atoms of the band B from the projection.(The Fermi levels are set to zero).

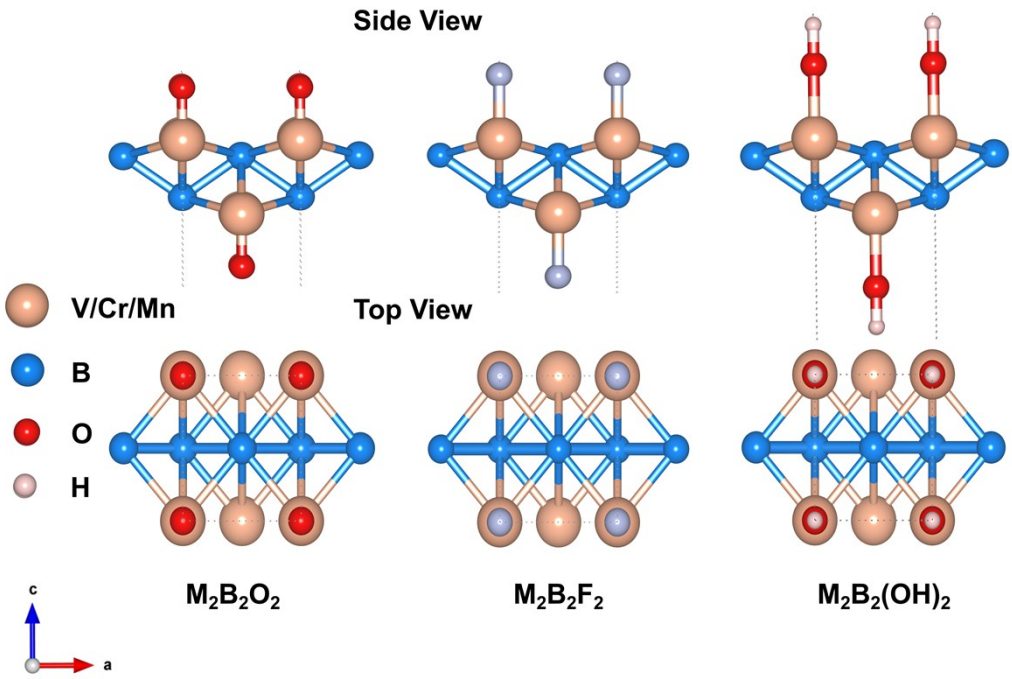

Fig. S6 Top and side views of the most stable configurations for functionalized MBenes $M_2B_2T_2$ (M is V/Cr/Mn, T is O, F, or OH).

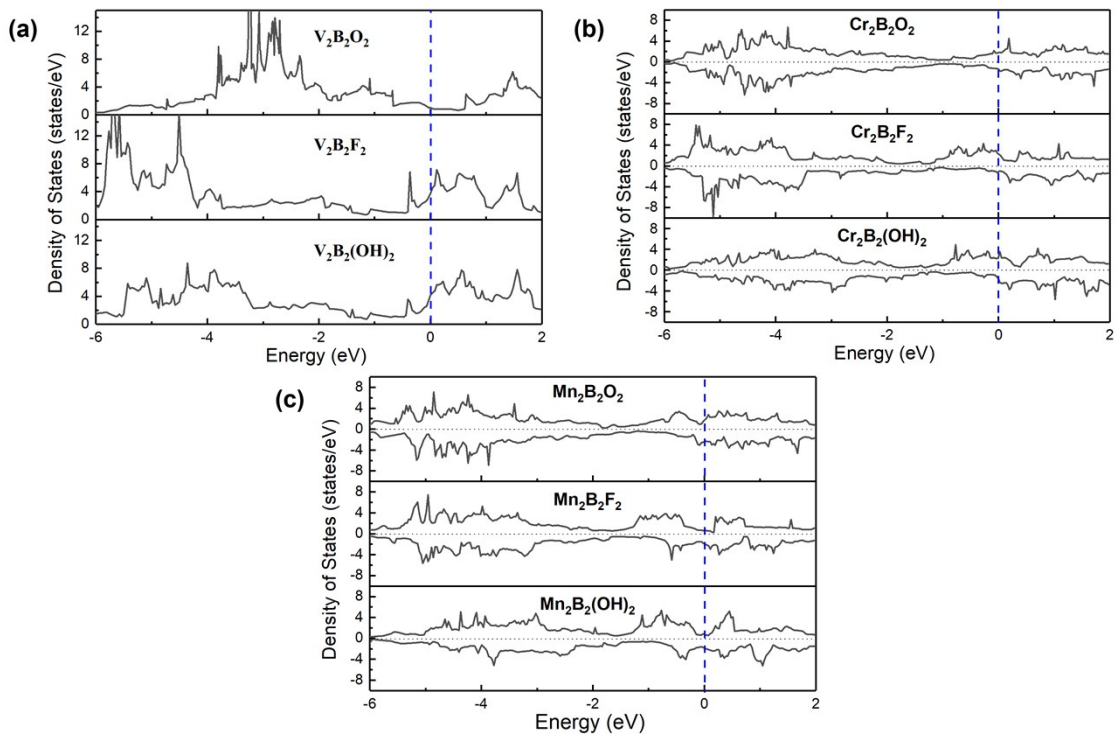

Fig. S7 DOS for functionalized MBenes $M_2B_2T_2$ (M is V/Cr/Mn, and T is O, F, or OH). The Fermi energy is set to 0 eV and indicated by the vertical dashed line.

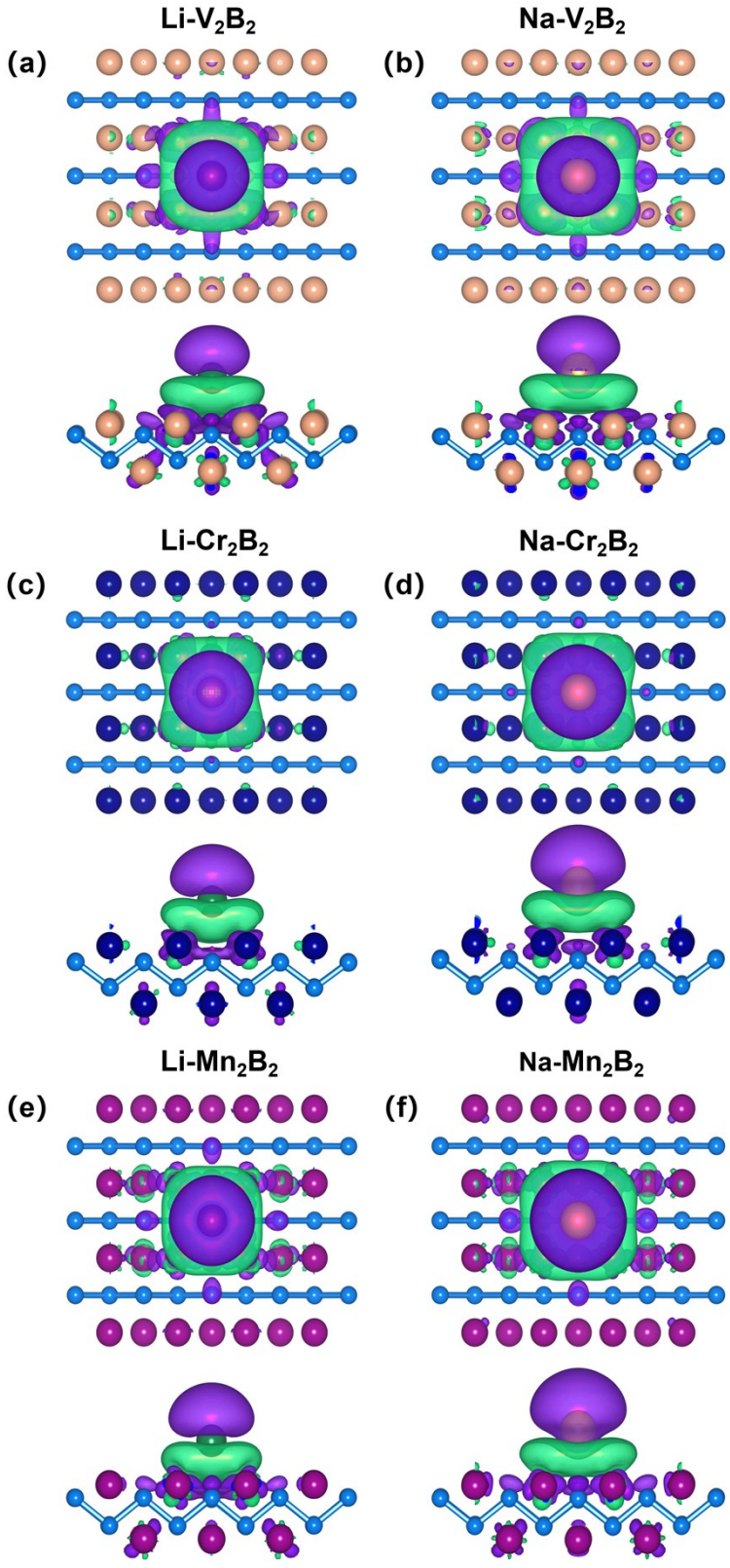

Fig. S8 Calculated charge density differences of MBenes (V_2B_2, Cr_2B_2, and M_2B_2) with one Li/Na atom adsorbed. Purple indicates charge accumulation, and green indicates charge depletion.

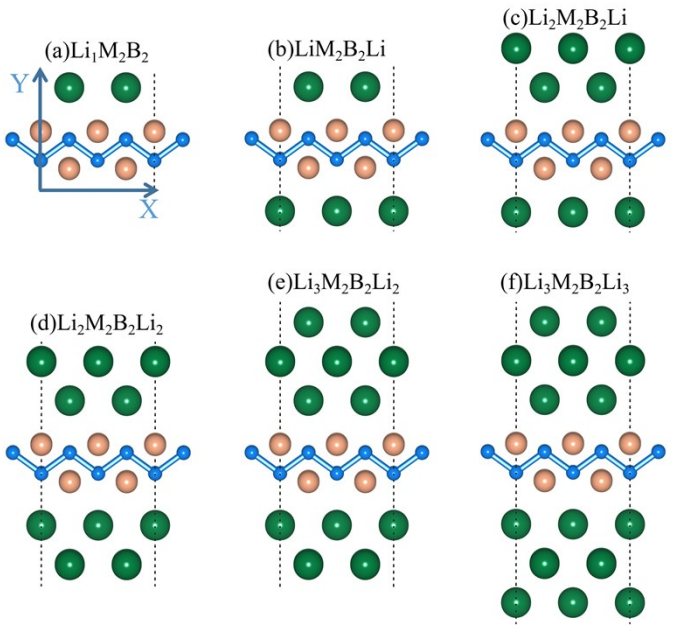

(g)

species	Lithium layer	Ead
V_2B_2	1	-0.548
V_2B_2	2	-0.309
V_2B_2	3	-0.162
Cr_2B_2	1	-1.237
Cr_2B_2	2	-0.903
Cr_2B_2	3	0.171
Mn_2B_2	1	-1.150
Mn_2B_2	2	-0.196
Mn_2B_2	3	0.092

Fig. S9 Calculation of the average Li atom adsorption energy on monolayer MBenes (V_2B_2, Cr_2B_2, and M_2B_2) with different adsorption layers.

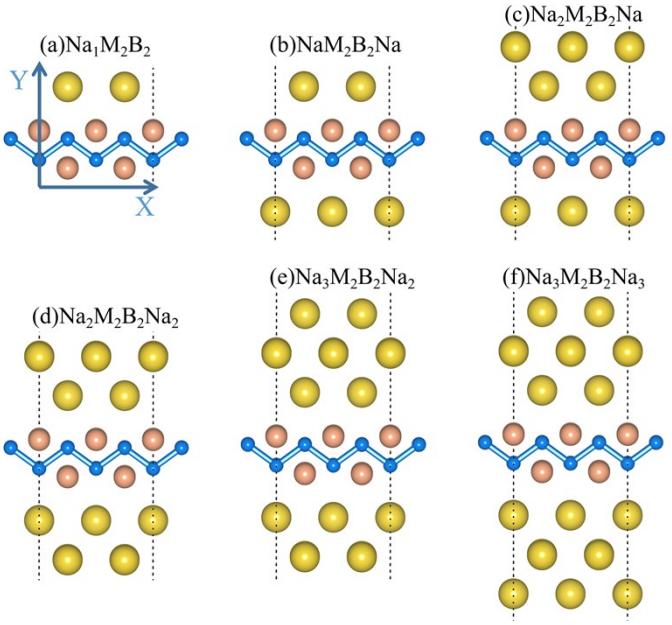

(g)

species	Lithium layer	Ead
V_2B_2	1	-0.432
V_2B_2	2	-0.276
V_2B_2	3	-0.093
Cr_2B_2	1	-0.855
Cr_2B_2	2	-0.135
Cr_2B_2	3	0.288
Mn_2B_2	1	-0.831
Mn_2B_2	2	-0.224
Mn_2B_2	3	0.040

Fig. S10 Calculation of the average Na atom adsorption energy on monolayer MBenes (V_2B_2, Cr_2B_2, and M_2B_2) with different adsorption layers.

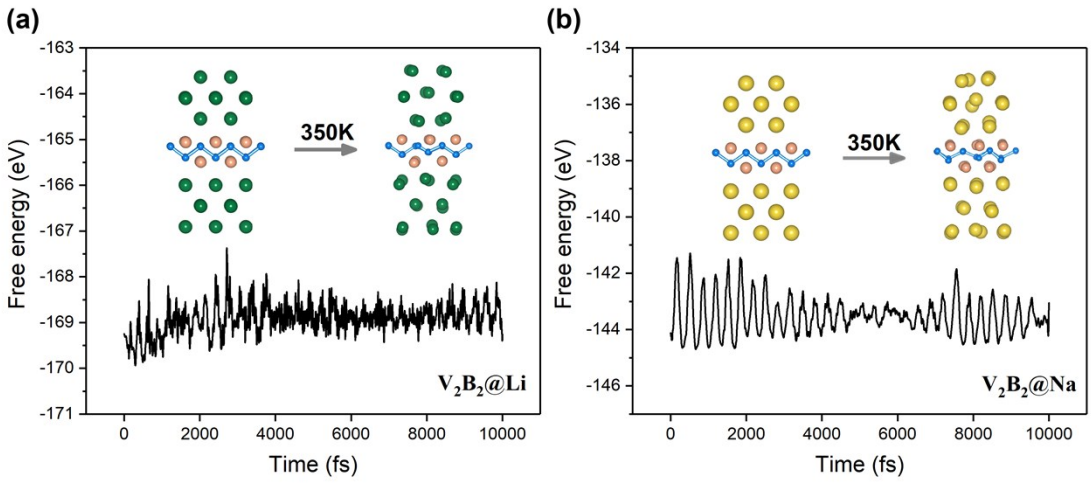

Fig. S11 Atomic structure of 2D V_2B_2 with adsorbed Li/Na in the AIMD simulation at 300 K after a time scale of 10 ps.

To verify the thermal stability of $M_3V_2B_2M_3$; M= (Li, Na), we perform AIMD simulations at 300 K using 3×3 supercells. After a 10 ps MD simulation, the free energy of $Li_3V_2B_2Li_3$ and $Na_3V_2B_2Na_3$ quickly reaches equilibrium (~1 ps) and fluctuates around the equilibrium value. The snapshot results show that all adsorbed metal atoms are slightly offset relative to their equilibrium position (Fig. S11). V_2B_2 in $Li_3V_2B_2Li_3$ and $Na_3V_2B_2Na_3$ exhibits only slight structural deformation compared to the bare V_2B_2 monolayer. When we remove all Li/Na atoms and reimplement the MD simulation, the distorted V_2B_2 can quickly recover its original configuration. MD simulations show that monolayer V_2B_2 has excellent stability during Li/Na ion insertion/extraction.

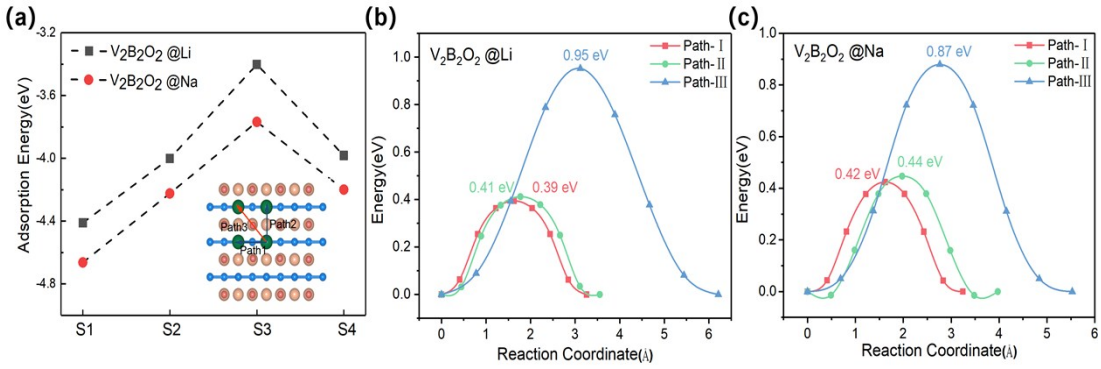

Fig. S12 (a) Calculated Li/Na ion adsorption energies at different locations on monolayer $V_2B_2O_2$, and schematic diagrams of the diffusion paths of the sites considering the diffusion energy barriers of (b) Li and (c) Na on the $V_2B_2O_2$ monolayer.

For the MBenes after functionalization, we studied the energy diffusion barriers on the $V_2B_2O_2$ surface for adsorbed Li/Na atoms. As shown in Fig. S12, the lowest diffusion energy barriers for Li/Na atoms on $V_2B_2O_2$ are 0.39 and 0.42 eV, which are higher than those on V_2B_2 (0.22 and 0.13 eV). The larger diffusion energy barriers for Li/Na atoms on the MBene indicate that O_2 functionalization generates large diffusion energy barriers, which is not conducive to the migration and diffusion of Li/Na atoms between sites.

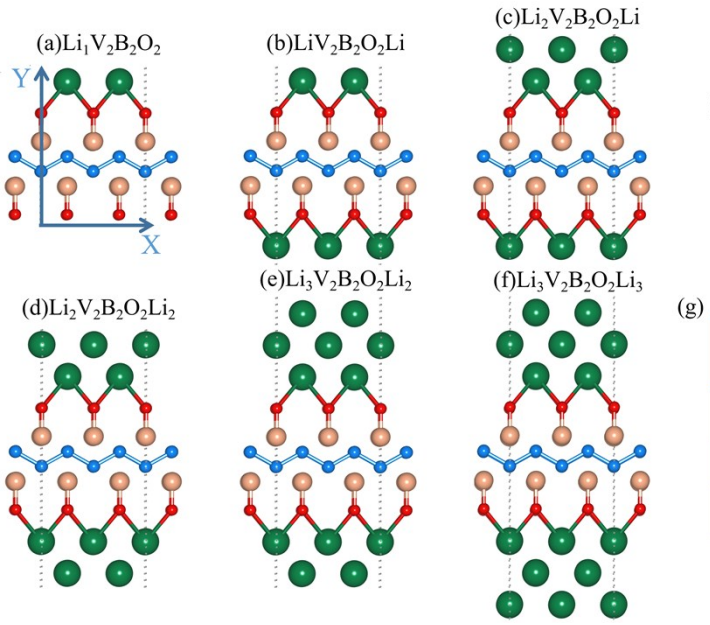

(g)

species	Lithium layer	Ead
$V_2B_2O_2$	1	-7.316
$V_2B_2O_2$	2	-3.937
$V_2B_2O_2$	3	-3.858

Fig. S13 Calculation of the average Li atom adsorption energy on monolayer $V_2B_2O_2$ with different adsorption layers.

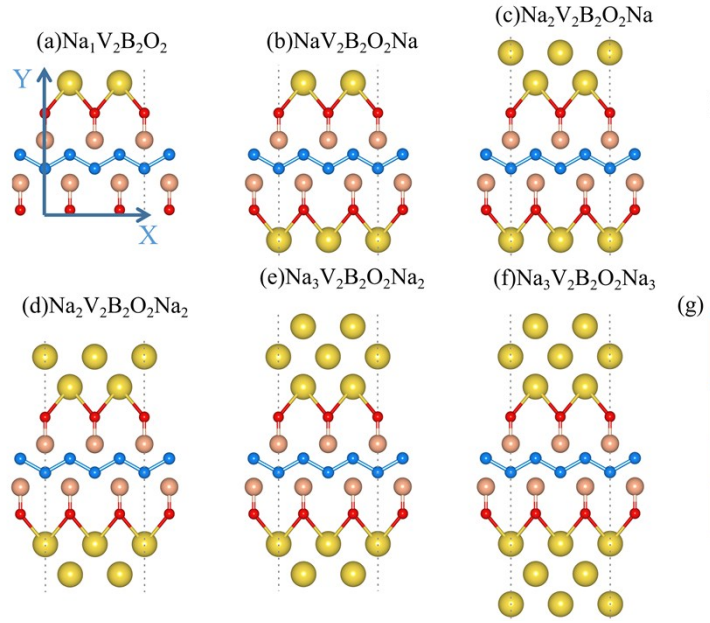

(g)

species	Lithium layer	Ead
$V_2B_2O_2$	1	-5.336
$V_2B_2O_2$	2	-2.684
$V_2B_2O_2$	3	-2.489

Fig. S14 Calculation of the average Na atom adsorption energy on monolayer $V_2B_2O_2$ with different adsorption layers.

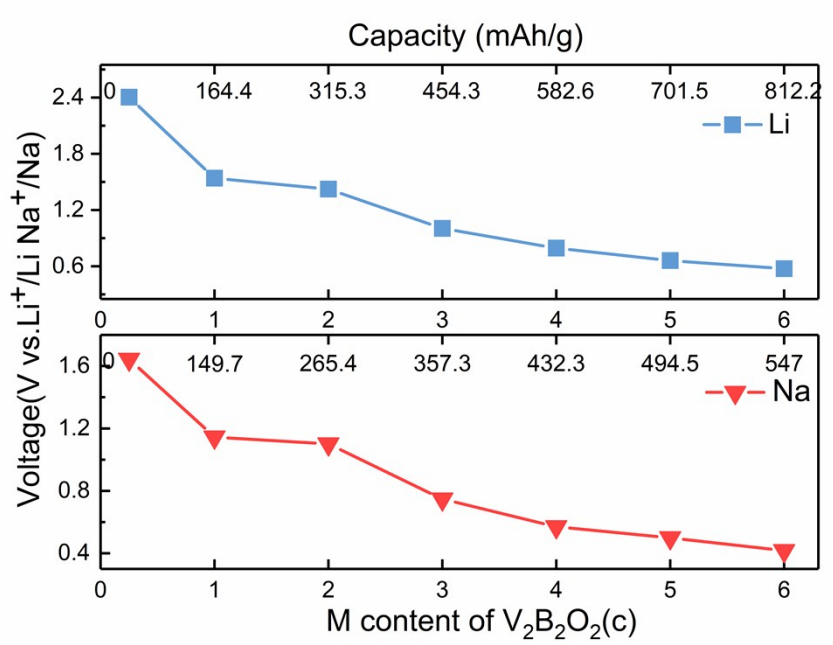

Fig. S15 Calculation of the specific capacity and voltage curves of $V_2B_2O_2$ monolayers under different Li and Na cation adsorptions.

Based on the calculated average adsorption energies of Li/Na atoms and their stable configuration, as shown in Figs. S13 and S14, the functionalized $V_2B_2O_2$ (2×2×1 supercell) can hold up to 24 Li/Na atoms without any structural distortion, corresponding to the $M_3/V_2B_2O_2/M_3$ (M=Li/Na) stoichiometry. The theoretical specific capacity and average OCV of monolayer $V_2B_2O_2$ are estimated to be 812 and 547 mA h g^{-1} and 0.57 and 0.41 eV, respectively, for lithium-ion batteries (LIBs) and sodium-ion batteries (NIBs).

Table legend

Lattic（Å）	a(cal.)	a(exp.)[6]	b(cal.)	b(exp.)[6]	c(cal.)	c(exp.)[6]
Cr_2AlB_2	2.923	2.937	2.933	2.968	11.043	11.051
2D Cr_2B_2	2.879		2.949			
Mn_2AlB_2	2.895	2.918	2.831	2.893	11.069	11.038
2D Mn_2B_2	2.883		2.932			
V_2AlB_2	3.011		3.075		11.111	
2D V_2B_2	2.900		3.267			
Ti_2AlB_2	3.047	-	3.310	-	11.322	-
2D Ti_2B_2	2.963		3.183			
Zr_2AlB_2	3.191	-	3.605	-	12.014	-
2D Zr_2B_2	3.082		3.291			
Nb_2AlB_2	3.157	-	3.331	-	11.674	-
2D Nb_2B_2	3.005		3.211			

Table S1 The calculated lattice parameters (Å) of 2D MBenes and bulk MABenes phases.

Table S2 The cohesive energy, magnetic moment M(pbe), bond length and slice thickness of Cr_2B_2, Mn_2B_2,V_2B_2,Ti_2B2,Zr_2B_2,and Nb_2B_2.

	Cr_2B_2	Mn_2B_2	V_2B_2	Ti_2B_2	Zr_2B_2	Nb_2B_2
Cohesive energy/ eV	5.870	5.374	5.460	4.681	4.984	6.018
Slice thickness/Å	0.112	0.096	0.099	0.161	0.186	0.171
Bond length/Å (d1)	2.160	2.119	2.225	2.314	2.483	2.357
(d2)	2.213	2.174	2.206	2.274	2.435	2.348
thickness	2.296	2.119	1.905	2.388	2.837	2.561
M / μB	4.68	4.71	0	0.06	0	0.02

Table S3 The calculated elastic constants (C_{ij}) for 2D V_2B_2, Cr_2B_2 and Mn_2B_2.

Systems	C_{11}/Gpa	C_{22}/Gpa	C_{12}/Gpa	C_{66}/Gpa
V_2B_2	227.03	93.98	74.01	79.86
Cr_2B_2	212.51	158.78	60.12	94.77
Mn_2B_2	198.58	149.80	60.31	88.42

For novel 2D materials, the mechanical properties are usually very striking. The elastic constants are the basis for evaluating the mechanical properties. According to the Born standard, a mechanically stable two-dimensional structure should satisfy $C_{11}C_{22} - C_{12}^2 > 0$ and $C_{44} > 0$. The elastic constants of MBenes are calculated from the strain energy versus strain curves, as shown in Table S3. Obviously, these results meet the Born-Huang criterion, and the materials are mechanically stable.

Table S4 The Young's modulus and Poisson's ratio of MBenes with some other 2D materials.

	Y_x(GPa.nm)	Y_y(GPa.nm)	V_x	V_y	ref
V_2B_2	169	70	0.79	0.33	This work
Cr_2B_2	189	141	0.38	0.28	This work
Mn_2B_2	174	131	0.40	0.30	This work
t-TiC	46	142	0.11	0.11	[7]
Ti_2C	121	130	0.26	0.23	[8]
Black Phosphorene	23.2	88.5	0.21	0.78	[9]
MoS_2	119		0.25		[10]
Graphene	342		0.17		[11]

The Young's moduli of MBenes are significantly larger than those of the MXenes Ti_2C, black phosphorene and 2D MoS_2. In summary, 2D MBenes are mechanically stable with isotropic and ultrahigh Young's modulus, which suggests their promise for applications such as a reinforcement in composites.

Table S5 Calculation of the change in the lattice parameters and volume during the intercalation/deintercalation process of LIBs/NIBs.

Bulk	a(Å)	b(Å)	Volume(Å)
V_2B_2	5.84	6.33	751.83
$Li_3V_2B_2Li_3$	5.88(0.68%)	6.25(1.2%)	724.81(3.59%)
$Na_3V_2B_2Na_3$	5.98(-2.39%)	6.47(-2.21%)	751.99(-0.02%)
Cr_2B_2	5.72	5.86	679.85
$Li_3Cr_2B_2Li_3$	5.75(-0.67%)	5.89(-0.64%)	690.42(-1.55%)
$Na_3Cr_2B_2Na_3$	5.85(-2.27%)	6.01(-2.56%)	693.46(-2.0%)
Mn_2B_2	5.72698	5.80	735.50
$Li_3Mn_2B_2Li_3$	5.76(-0.69%)	5.86(-1.10%)	747.94(-1.69%)
$Na_3Mn_2B_2Na_3$	5.80(-1.28%)	5.81(-0.17%)	746.27(-1.46%)

A new electrode material is usually affected by the large volume fluctuations during lithiation/sodiation in actual usage. Therefore, the lattice constant and volume change percentages during lithiation/sodiation are also important indices for evaluating the structural stability/integrity of electrode materials. Table S5 shows the changes in the lattice constant $\Delta C/C_0$ in the process of lithiation/sodiation, where C and C_0 are the lattice constants of the lithium/sodium-doped and original MBenes. Li and Na doping leads to maximum expansion and shrinkage of ~1.2% and 2.56%. The slightly larger expansion with Na addition is due to its higher van der Waals radius. More importantly, the volume expansion and shrinkage does not exceed 4% during lithiation/sodiation of MBenes, and this small volume change is very beneficial to the cycling performance of LIBs and NIBs. In view of these results, monolayer MBenes can be stably used as anode materials in LIBs and NIBs.

Table S6 Theoretical specific capacity and diffusion energy barriers of the currently widely studied LIB anode materials.

Species	Theoretical specific capacity	Diffusion barrier	Electronic Conductivity	Ref
V_2B_2	969	220	Metallic	This work
Cr_2B_2	696	280	Metallic	This work
Mn_2B_2	679	290	Metallic	This work
MoS_2	600	210	Semiconducting	[12]
Graphite	372	450–1200	Metallic	[13, 14]
Graphene	744	350-520	Semiconducting	[15]
Silicene	957	230–600	Semiconducting	[16]
1T-Ti_3C_2	448	70	Metallic	[17]
1H-Mo_2C	526	35	Metallic	[18]
1T-Ti_2C	160	20	Metallic	[19]
Orthorhombic Fe_2B_2	665	240	Metallic	[20]
Orthorhombic Mo_2B_2	444	270	Metallic	[20]

To more fully evaluate the potential of monolayer MBenes as LIB/NIB anode materials, we compare their theoretical specific capacity and diffusion potential with those of other widely studied anode materials. As shown in Table S6, the theoretical specific capacities of the monolayer MBenes V_2B_2, Cr_2B_2, and Mn_2B_2 are 969, 696, and 679 mA h g^{-1}, respectively, which are greater than those of common graphite, MoS_2, and silicene. Compared with the same type of two-dimensional Mxene, the MBenes show an advantage in terms of the theoretical

capacities but a disadvantage in terms of the diffusion energy barriers, which are lower than those of Ti_3C_2, Mo_2C, and Ti_2C. Doping with cations is expected to improve the lithium-ion migration rate in the future.

Table S7 Theoretical specific capacity and diffusion energy barriers of the currently widely studied NIB anode materials.

Species	Theoretical specific capacity	Diffusion barrier	Electronic conductivity	Ref
V_2B_2	614	130	Metallic	This work
Cr_2B_2	492	170	Metallic	This work
Mn_2B_2	483	170	Metallic	This work
MoS_2	146	280	Semiconducting	[21]
Ti_3O_7	210	190	Metallic	[22]
Ti_3C_4	560	350	Metallic	[23]
$Zr_3C_2O_2$	325	290	Metallic	[24]
Boron phosphide	143	220	Metallic	[25]

In sodium-ion battery applications, as shown in Table S7, the theoretical specific capacities of the monolayer MBenes V_2B_2, Cr_2B_2, and Mn_2B_2 are 614, 492, and 483 mA h g^{-1}, which are larger than those of common MoS_2, Ti_3O_7, $Zr_3C_2O_2$ and boron phosphide and close to the reported Ti_3C_4 capacity. The diffusion energy barrier (130 meV) for Na ions on monolayer V_2B_2 is much lower than that on any of the other typical promising anode materials shown in Table S7, indicating a very high rate performance.

References:

1. H. Zhang, Y. Li, J. Hou, K. Tu and Z. Chen, *J Am Chem Soc*, 2016, **138**, 5644-5651.

2. A. Togo, F. Oba and I. Tanaka, *Physical Review B*, 2008, **78**.

3. G. J. Martyna, M. L. Klein and M. Tuckerman, *The Journal of chemical physics*, 1992, **97**, 2635-2643.

4. C. Lee, X. Wei, J. W. Kysar and J. Hone, *Science*, 2008, **321**, 385-388.

5. J. Lu, S. Kota, M. W. Barsoum and L. Hultman, *Materials Research Letters*, 2016, **5**, 235-241.

6. J. Greeley, T. F. Jaramillo, J. Bonde, I. Chorkendorff and J. K. Nørskov, *Nature Materials*, 2006, **5**, 909-913.

7. Z. Zhang, X. Liu, B. I. Yakobson and W. Guo, *Journal of the American Chemical Society*, 2012, **134**, 19326-19329.

8. S. Wang, J.-X. Li, Y.-L. Du and C. Cui, *Computational Materials Science*, 2014, **83**, 290-293.

9. Q. Wei and X. Peng, *Applied Physics Letters*, 2014, **104**, 251915.

10. J. Deng, I. Fampiou, J. Z. Liu, A. Ramasubramaniam and N. V. Medhekar, *Applied Physics Letters*, 2012, **100**.

11. R. C. Andrew, R. E. Mapasha, A. M. Ukpong and N. Chetty, *Physical Review B*, 2012, **85**.

12. X. Chen, J. He, D. Srivastava and J. Li, *Applied Physics Letters*, 2012, **100**.

13. S. Thinius, M. M. Islam, P. Heitjans and T. Bredow, *The Journal of Physical Chemistry C*, 2014, **118**, 2273-2280.

14. R. Yazami and P. Touzain, *Journal of Power Sources*, 1983, **9**, 365-371.

15. H. Zhang, Y. Xia, H. Bu, X. Wang, M. Zhang, Y. Luo and M. Zhao, *Journal of Applied Physics*, 2013, **113**, 044309.

16. G. A. Tritsaris, E. Kaxiras, S. Meng and E. Wang, *Nano Letters*, 2013, **13**, 2258-2263.

17. D. Er, J. Li, M. Naguib, Y. Gogotsi and V. B. Shenoy, *ACS Applied Materials & Interfaces*, 2014, **6**, 11173-11179.

18. Q. Sun, Y. Dai, Y. Ma, T. Jing, W. Wei and B. Huang, *The Journal of Physical Chemistry Letters*, 2016, **7**, 937-943.

19. S. Zhao, W. Kang and J. Xue, *The Journal of Physical Chemistry C*, 2014, **118**, 14983-14990.

20. Z. Guo, J. Zhou and Z. Sun, *Journal of Materials Chemistry A*, 2017, **5**, 23530-23535.

21. M. Mortazavi, C. Wang, J. Deng, V. B. Shenoy and N. V. Medhekar, *Journal of Power Sources*, 2014, **268**, 279-286.

22. H. Pan, X. Lu, X. Yu, Y.-S. Hu, H. Li, X.-Q. Yang and L. Chen, *Advanced Energy Materials*, 2013, **3**, 1186-1194.

23. Q. Meng, A. Hu, C. Zhi and J. Fan, *Physical Chemistry Chemical Physics*, 2017, **19**, 29106-29113.

24. Q. Meng, J. Ma, Y. Zhang, Z. Li, A. Hu, J.-J. Kai and J. Fan, *Journal of Materials Chemistry A*, 2018, **6**, 13652-13660.

25. H. R. Jiang, W. Shyy, M. Liu, L. Wei, M. C. Wu and T. S. Zhao, *Journal of Materials Chemistry A*, 2017, **5**, 672-679.